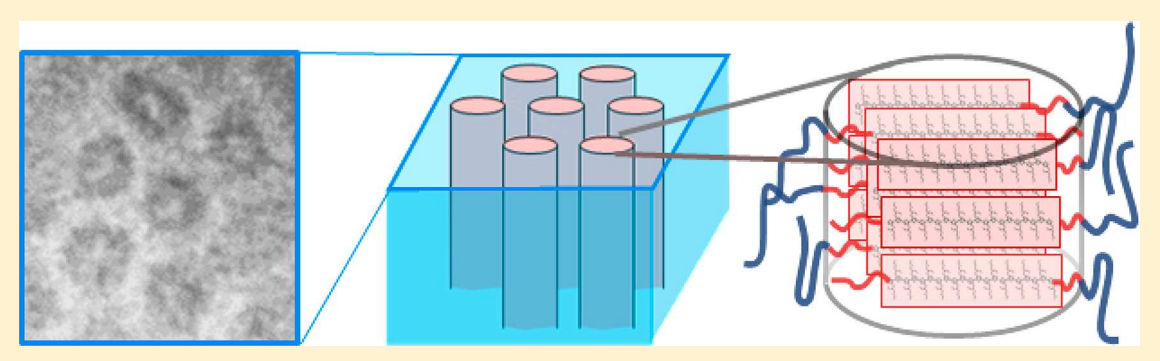
Macromolecules

Confined Crystallization within Cylindrical P3EHT Block Copolymer **Microdomains**

Emily C. Davidson[†] and Rachel A. Segalman*,^{†,‡}

[†]Department of Chemical Engineering and [‡]Materials Department, University of California, Santa Barbara, Santa Barbara, California 93106, United States

Supporting Information



ABSTRACT: Confinement of crystallites within block copolymer microdomains is a promising approach to study conjugated polymer crystallization due to interfacial chain tethering and defined geometries. The nanoscale organization of crystallites is often critical to determining the charge transport properties of conjugated polymers. Here, a poly(3-(2'-ethyl)hexylthiophene)block-poly(methyl acrylate) (P3EHT-b-PMA) system is leveraged to study the impact of confinement within cylindrical microdomains. The crystalline P3EHT permits accessible melting temperatures and robust formation of traditional microphaseseparated morphologies, while the rubbery PMA allows the local deformations required to permit P3EHT crystallization. Crystallites form with chains perpendicular to the diblock interface, causing domain expansion; TEM reveals that this is accommodated in the cylindrical geometry via local deformation. Complementary SAXS/WAXS of aligned diblocks shows preferential orientation of the alkyl chain stacks down domains. Furthermore, cylindrically confined P3EHT demonstrates a smaller window of thermal control over crystalline perfection via isothermal crystallization conditions than homopolymer P3EHT or block copolymer P3EHT in lamellar confinement. This work demonstrates that postcrystallization annealing is an alternative route to generating uniformly high quality crystallites in cylindrically confined P3EHT. These results are important for considering routes to optimizing and controlling crystallinity in nanoscale confined geometries.

■ INTRODUCTION

Conjugated polymers have been applied to light-emitting diodes, solar cells, and transistors which rely crucially on charge mobility. 1-3 In these materials, charge mobility is highly influenced by structural details of the resulting crystallinityparticularly crystalline orientation—as influenced by factors including confinement, ⁴⁻⁷ processing conditions, ⁸⁻¹² mechanism of crystallization, ¹³⁻¹⁷ and details of molecular design and architecture. ^{14,18,19} The study of confinement within controlled geometries and tethering of chain ends presents a unique opportunity to template and control conjugated polymer crystallization. In particular, microphase-separated diblock copolymers present a model system in which confinement geometry and curvature may be controlled to understand their impacts upon the resulting polymer crystallization. Ultimately, this allows us to understand more deeply the mechanism of crystallite growth in conjugated polymers, the forces impacting preferred crystallite growth directions, and the limits of how curved geometries may accommodate extended-chain crystallites. These details have important implications for how conjugated polymer crystallinity can be controlled as well as the ability of these confined crystallites to transport charge.

Conjugated polymers tend to have high melting points, which are associated with close π -stacking which enables interchain charge transport. However, when these conjugated polymers are incorporated into diblock copolymer systems, these high melting points typically cause crystallization to dominate self-assembly. Poly(3-(2'-ethyl)hexylthiophene) features accessible melting temperatures, while maintaining key features of the many more extensively studied conjugated polymers.^{27–30} In particular, P3EHT in block copolymers leads to robust formation of microphase-separated morphologies and maintains them following crystallization.³¹ In lamellar diblock copolymer confinement, the P3EHT crystallite orientation is templated relative to the diblock interface. Furthermore, conjugated polymer chains demonstrate a driving force to

Received: June 21, 2017 Revised: July 25, 2017 Published: August 9, 2017



extend upon crystallization and drive domain expansion during crystallization.³² Surprisingly in these lamellar systems, confinement does not appear to significantly impact the stability of the resulting crystallite populations; P3EHT melting points remain comparable to the constitutive homopolymers. Furthermore, charge mobilities of P3EHT in diblocks measured via time-of-flight remain comparable to those of the constitutive homopolymers.³¹

Cylindrical geometries are of interest as a template for organic photovoltaics or as a model system for controlled charge transport in one dimension. However, these geometries present new challenges to the confined crystallization of conjugated polymers. While the lamellar system adopts uniaxial symmetry in-plane (π - π and alkyl chain stacking are both inplane),³² the question remains of what crystallite growth direction is preferred along the long axis of the cylinders. Notably, in the homopolymer, long crystalline "fibrils" form with the $\pi - \pi$ stack along the long axis. Interestingly, crystallization-driven self-assembly of P3HT diblocks, while lacking the long-range order of diblocks microphase separated in the melt, features locally fibrillar morphologies similar to the homopolymer. 17,20 By contrast, model studies of P3HT crystallized within anodized alumina nanopores displayed diameter-dependent orientation: at large diameters (above 120 nm), the π - π stacking was found to run parallel to the cylinder long axis, while at small diameters (50-15 nm) the orientation with π - π direction perpendicular to the cylinder long axis began to predominate; the authors hypothesize that at small diameters local nucleation from the edge of the pore walls dominates the crystallization mechanism and results in the change in orientation.³³ However, in this case, nucleation from the diblock interface is unexpected; since conjugated polymers are typically characterized by strong π – π stacking interactions that drive crystallization, it was expected that the $\pi-\pi$ interactions would dominate along the length of the cylinder. Essentially, this orientation would result in a "fibril" within a microphase templated cylinder. Importantly, the resulting orientation is critical for determining the potential material applications given that charge transport with crystallites is fastest along the chain backbone and slowest in the alkyl chain stacking direction. Furthermore, while the impact of confined crystallization within cylindrical geometries on templated crystallite orientation and crystallization kinetics have been studied in traditional flexible polymers, 34-37 new competing preferences arise in conjugated systems. In the cylindrical microdomains it is clearly impossible for all conjugated chains both to participate in extended-chain crystallites and to orient perpendicular to domains, raising the question of how crystallization within the microdomains will attempt to satisfy these conflicting demands.

The mode of crystallization and the stability of the resulting crystallites may also be impacted by confinement. 37–39 Previous works studying the nucleation mechanism of flexible polymers in confinement have noted either a shift from a heterogeneous to a homogeneous nucleation mechanism or reduced degrees of crystallinity attributed to glassy walls arresting the mobility of tethered crystalline chains. 39–43 Such shifts in nucleation mechanism could require critical changes in material processing conditions to achieve high quality crystallites within these nanostructured conjugated polymers. Importantly, this dramatic shift in mechanism is not necessarily expected within conjugated polymers. Standard crystalline homopolymers are composed of micrometer-scale spherulites; these are known to

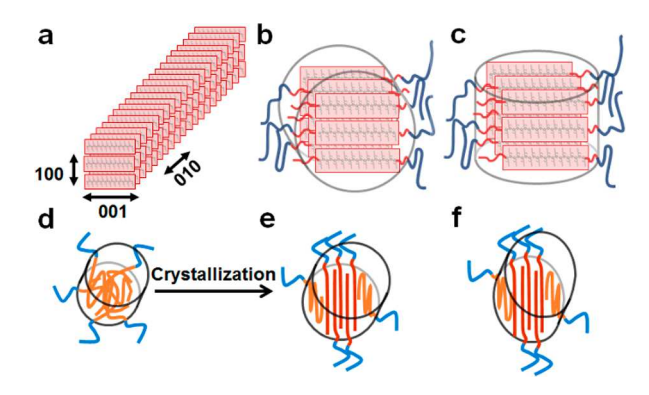


Figure 1. Possible ways crystalline P3EHT may be accommodated within cylindrical microdomains. (a) P3EHT is known to form fibrils with P3EHT π -stacking down the long axis; the orientation of crystals in (b) would allow P3EHT to crystallize with long-range π -stacking similar to a fibril down the center of the cylinder. The orientation in (c) is also possible, with alkyl chain stacking down the long-axis of the cylinder. (d) P3EHT-*b*-PMA cylinders in the melt easily accommodated relaxed P3EHT chains. P3EHT undergoes crystallization with concurrent increase in the apparent size of cylinders. Extended-chain P3EHT crystallites may be accommodated by (e) the entire domain expanding, with some amorphous material excluded at the edges, or (f) deformation of domains.

follow a heterogeneous nucleation mechanism characterized by one nucleation site (typically attributed to dust or other defects) per spherulite.⁴⁴ Thus, a decrease in cylinder volume below the length scales of the typical nucleation site distribution induces a fundamental change in nucleation mechanism.³⁸ By contrast, conjugated polymers readily aggregate driven by π - π interactions. When these aggregates are sufficiently well-ordered and large in size, they are considered crystalline and form fibrillar crystals with dimensions of approximately 15 nm in diameter and order of 200 nm in length; assuming a single nuclei per fibril, this result implies a typical nucleation density on the order of the volume of a cylindrical microdomain. 12,45 Thus, it is expected that the cylindrical microdomains will have a comparable nucleation density to P3EHT homopolymer; a change in nucleation mechanism is not necessarily anticipated. However, the tethering of P3EHT chains to the edges of crystallites is expected to, similar to the lamellar system, dramatically slow the crystallization dynamics.

This work examines P3EHT crystallization confined within cylindrical microdomains and seeks to understand how the shift from lamellar to cylindrical confinement impacts the resulting crystallinity. In particular, the impact of cylindrical geometry on crystallite orientation is investigated, revealing that—surprisingly—crystallites orient with the alkyl chain stacking direction along the long axis and π -stacking across the short axis. Further, lateral expansion of domains upon crystallization (despite densification of the P3EHT) emphasizes that conjugated chains preferentially extend upon crystallization; imaging studies via TEM find that curved domains accommodate crystallites composed of extended chains via local anisotropic deformation. Finally, since the impact of confinement on the crystallization dynamics and stability is critically important for developing processing methods leading to property optimization, the melting behavior is investigated as a function of time, temperature, and degree of confinement. Crystallization kinetics are limited—in particular at high temperature—at small volume fractions relative to in lamellar confinement,

Table 1. Molecular and Morphological Characteristics of P3EHT-b-PMA Cylinder Forming Diblocks

P3EHT-b-PMA composition	Ð	$arphi_{ ext{mel} v}$ P3EHT	contour length, P3EHT (nm)	cylinder diameter, melt ^a	cylinder diameter, crystalline ^a	T _g (°C), PMA	$T_{\rm m}$ (°C), P3EHT recrystallized at 65 °C
8.3k/14.9k	1.23	0.38	16.6	12.8	14.9	7.6	84.3
8.3k/31.2k	1.24	0.21	16.6	11.3	11.8	6.3	84.5
11.1k/20.6k	1.19	0.33	22.3	14.6	19.8	5.5	83.2

[&]quot;Cylinder diameters calculated from hexagonally packed cylinder geometry and melt and crystalline volume fractions. Crystalline diameter assumes a crystalline P3EHT density of 1.10 g/cm³.

implying a potential change of nucleation mechanism. Importantly, while in lamellar confinement the manipulation of crystallization temperature permits manipulation of the degree of crystalline perfection, the range of accessible crystallization temperatures is smaller in cylindrical confinement. This work shows that despite this limited range the P3EHT melt-recrystallization mechanism can be manipulated to produce crystallites with high and uniform melting points via annealing.

EXPERIMENTAL SECTION

Synthesis. Reagents and solvents used as received from Sigma-Aldrich unless otherwise noted. P3EHT monomer, end-functionalized polymer, and diblocks were synthesized as previously described. ^{30,32}

Molecular Characterization. Molecular weights and dispersity according to PS standards were determined via gel permeation chromatography (GPC) on a Waters instruments using a refractive index detector and Agilent PLgel 5 μ m MiniMIX-D columns (GPC traces in SI Figure 1). THF at 35 °C was used as the mobile phase with a flow rate of 0.3 mL/min. 1 H NMR spectra were collected on a Bruker AV-500 MHz spectrometer and on a Varian VNMRS 600 MHz spectrometer using deuterated chloroform (Cambridge) as the solvent with \sim 1 wt % polymer. Reported molecular weights are by end-group analysis. Densities were collected via gas pycnometry (P3EHT) 32 or are calculated from the literature (PMA 46 and PS 47).

SAXS/WAXS. Both aligned and isotropic samples for X-ray scattering were prepared. Isotropic samples were melt-pressed into 1 mm thick aluminum washers at 150 °C while aligned strips were created with a channel flow die. 48 Material is initially loaded into the center of the die (a long, flat channel with walls on either side). Upon compressing a top part onto the channel, the sample flows out away from the load position (in the "flow direction") but is constrained by the walls ("constraint direction") in addition to the top/bottom of the channel ("load direction").48 Samples were isothermally crystallized for one week within temperature-controlled ovens prior to data collection. For annealing studies, samples were annealed overnight following crystallization. SAXS and WAXS patterns were collected at beamline 7.3.3 of LBNL's Advanced Light Source (ALS) and beamlines 1-5 and 11-3 of the Stanford Synchrotron Radiation Lightsource (SSRL). Scattering patterns were calibrated against silver behenate (AgBe).⁴⁹ Scattering intensity is plotted versus the momentum transfer vector $q = (4\pi/\lambda) \sin \theta$. Scattering data were reduced using the Nika package for Igor Pro. 50

TEM. Samples for TEM were prepared by melt pressing polymer at 150 °C between two sheets of Kapton or Teflon followed by isothermal crystallization in temperature-controlled ovens for one week. The 100 nm thick thin sections for TEM were sliced from these samples using a Leica UC7 Ultramicrotome with FC7 cryo attachment. P3EHT-b-PMA samples were cryomicrotomed at $-25\,^{\circ}\mathrm{C}$ and collected directly from the dry diamond knife. Thin sections were placed on CF300 amorphous carbon coated Cu grids from Electron Microscopy Sciences. Sections were stained by 20 min exposure to RuO4 (2% aqueous RuO4 solution, Electron Microscopy Sciences) vapor. Imaging was performed on an FEI Tecnai G2 Sphera microscope operating at 200 kV.

DSC. Differential scanning calorimetry (DSC) measurements were performed using a TA Q2000 calorimeter. Samples (2–10 mg each) were hermetically sealed inside TZero aluminum pans. Samples in

pans were heated to 150 °C offline, held for 10 min to clear thermal history, and then isothermally crystallized for one week in temperature-controlled ovens. For annealing studies, samples were first crystallized for one week at room temperature and then annealed overnight at the desired temperature in temperature-controlled ovens. Samples were heated from -20 to 150 °C at 10 °C/min to observe both the PMA glass transition at $\sim\!10$ °C and P3EHT melting transitions at $\sim\!60\!-\!90$ °C. Melting points varied with crystallization and annealing conditions; glass transition temperatures and melting points following crystallization at 65 °C are reported in Table 1.

■ RESULTS AND DISCUSSION

Three cylinder-forming diblock copolymers containing a semiflexible P3EHT conjugated block and flexible PMA rubbery block were utilized to study conjugated polymer crystallization within curved geometries (Figure 1). Notably, PMA is highly distinct from PMMA; removing the backbone methyl group to form PMA decreases the glass transition from \sim 120 to \sim 10 °C. Here, the rubbery PMA block was chosen because prior studies in lamellar-forming diblocks demonstrated that a rubbery second block is critical for permitting the chain reorganization necessary for crystallization (namely, local chain extension in addition to P3EHT densification upon crystallization).³² Interestingly, the cylinder-forming composition window studied here (minority semiflexible P3EHT; P3EHT confined within cylinders) is favored over the opposite composition window (majority semiflexible P3EHT). Importantly, all cylinder-forming diblocks demonstrated crystallization with the same unit cell as homopolymer and lamellarconfined P3EHT. Here, the cylindrical geometry imposes unique constraints upon the crystallization. In particular, the volume of each continuously connected region in cylindrical geometries is clearly smaller than in lamellar confinement and is expected to result in less stable (lower-melting) crystallites and slower nucleation processes. Additional constraints appear initially contradictory; from simple packing considerations, the polymer clearly cannot both allow all chains to extend upon crystallization and maintain a circular geometry.

P3EHT-*b***-PMA Forms Cylindrical Morphologies Confining P3EHT.** In designing block copolymers containing functional materials for targeted morphology-dependent applications, it is critical to consider how the relative chain shape and stiffness of the blocks impact the resulting phase behavior. Here, the P3EHT-*b*-PMA system displays asymmetric phase behavior, strongly favoring lamellar morphologies at high volume fractions of P3EHT ($\phi_{\text{P3EHT}} = 0.46$ to $\phi_{\text{P3EHT}} = 0.67$). Meanwhile, over a composition window from $\phi_{\text{P3EHT}} = 0.12$ to $\phi_{\text{P3EHT}} = 0.39$, the system confines P3EHT within cylindrical morphologies. P3EHT and other poly(3-alkylthiophenes) are considerably stiffer than traditional flexible polymers with persistence lengths on the order of 3 nm. ^{51,52} By contrast, poly(methyl acrylate), used here, has a persistence length of only 0.74 nm. ⁵³ At moderate molecular weights of ~10kDa P3ATs display contour lengths on the order of 20 nm,

emphasizing that the chain conformation in the melt is still well-described by a random walk. These differences in chain stiffness can be parametrized in terms of a conformational asymmetry parameter, ε

$$\varepsilon = (\beta_{\rm A}/\beta_{\rm B})^2$$

that describes the differences in both conformational and volume-filling characteristics. ^{54,55} Here, $\beta^2 = R_g^2/V$, where R_g is the radius of gyration and V is the volume of the block. Importantly, even two polymers with chain conformations welldescribed by random walk statistics but with different persistence lengths will have considerably different volumefilling characteristics. Thus, significant degrees of conformational asymmetry can arise purely from a difference in local chain stiffness. Seen here, the difference in persistence length leads to conformational asymmetry that induces the observed composition window where curved interfaces are favored at high fractions of the more flexible block. 56-58 Importantly, the impacts of conformational asymmetry on self-assembly should not be confused with the impacts of liquid crystalline and crystalline interactions. While liquid crystalline interactions can induce smectic and nematic block copolymer phases in some systems, 59,60 and the competition between enthalpy-driven microphase separation and crystallization can lead to crystallization-dominated morphologies, ⁶¹ the simple difference in stiffness between chains in a molten diblock—described via conformational asymmetry—can lead to significant shifts in the composition window over which each morphology is favored.

Importantly, this behavior highlights key design rules for the self-assembly of conjugated-amorphous block copolymers. In particular, it highlights that chain stiffness does not merely impact liquid crystalline and crystalline behavior. For targeting specific morphologies in the melt it is also critical to consider the impact of local chain conformation on the block copolymer phase diagram. Here, we specifically examine three cylinderforming compositions within this window to understand the impact of P3EHT volume fraction and crystallization conditions on the resulting P3EHT crystallinity, finding that cylinders promote a crystallite orientation with alkyl chain stacking along the long axis and and at small volume fractions results in inaccessibly slow kinetics at temperatures previously used to manipulate the degree of crystalline perfection. Characteristic SAXS patterns (Figure 2) identify the diblocks which form curved interfaces; cylindrical morphologies are further confirmed via transmission electron microscopy (Figure

P3EHT Crystallization Induces Local Domain Deformation. The cylindrical microdomains and initial morphology are formed here in the melt, but ultimately the rubbery matrix permits deformation during the course of crystallization. Similar to lamellar morphologies, the diameter of P3EHT cylinders clearly increases upon crystallization despite densification of P3EHT (Table 1), emphasizing that the drive for chain extension is a key driving force during cylindrically confined crystallization. However, the average diameter of each cylinder does not approach the full contour length of the P3EHT block, indicating that either chains are not fully extended or domains do not experience uniform deformation due to local frustrations. Clearly, to accommodate extended conformations, the fraction of polymer chains capable of participating in the crystallite without completely disrupting the microdomain morphology is limited relative to the lamellar case. In order to

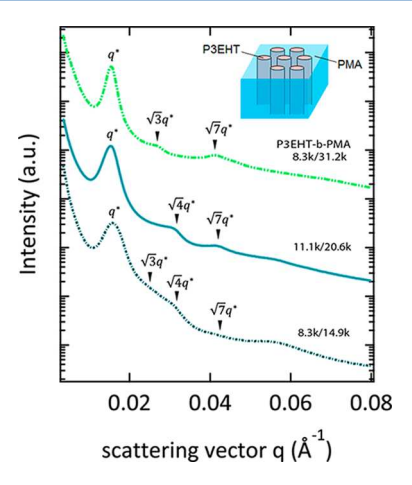
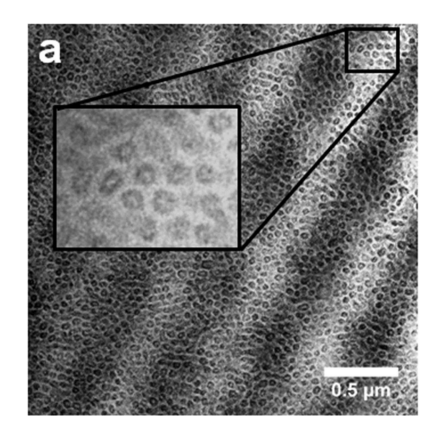


Figure 2. Small-angle X-ray scattering shows that P3EHT-*b*-PMA diblocks form cylindrical morphologies.

directly probe the deformation and understand how domains accommodate the chain extension, crystallites and microdomains were visualized via TEM. By selectively staining thin sections of crystallized cylinder-forming diblocks with RuO4, TEM imaging clearly defines the difference between noncrystalline regions (where staining agent diffuses quickly) and crystalline regions (where staining agent diffuses more slowly).⁶² The difference in contrast between unstained and selectively stained P3EHT-b-PMA is clear in SI Figure 2. Distinguishing the actual shape of the interior crystallites is challenging, but upon crystallization the resulting crystallites and microdomains are clearly not perfectly round, especially in the case (Figure 2a) of relatively high volume fractions of P3EHT. P3EHT-b-PS cylinders, by contrast, display no such deformation; staining and direct imaging yields no imagines of crystallites (SI Figure 3) and supports DSC results which demonstrate the lack of crystallinity in these systems. These deformed microdomain shapes in P3EHT-b-PMA crystallized cylinder-formers imply that these extended-chain crystallites are achieved through limited local deformation of the microdomains. Interestingly, while some chains can easily participate in these crystallites while maintaining a perpendicular orientation relative to the microdomain interface, other chains must either remain excluded or accommodate a significant conformational bend near the microdomain interface in order to participate in the crystallite.

Preferential Orientation of P3EHT within Cylindrical Microdomains. The preferred orientation of the resulting crystallites within microdomains is expected to have significant implications for potential applications. Charge transport along chains is fastest along the chain backbone, and charge transport between chains is facilitated by π -stacking. Therefore, the relative orientation of crystallites within microdomains determines how well charge can be transported down a domain. The incorporation of alkyl side chains in P3ATs is typically considered a necessary trade-off between performance and processability; while alkyl side chains permit solvent and thermal processing of the intractable polythiophene backbone, they are known to cause P3AT crystallites to be more resistive along the alkyl chain stacking direction.⁶³ While SAXS studies establish that cylinders expand upon crystallization, and TEM shows that this expansion is anisotropic, these studies do not uniquely identify the preferred crystallite orientation within the microdomains. To identify this orientation, complementary



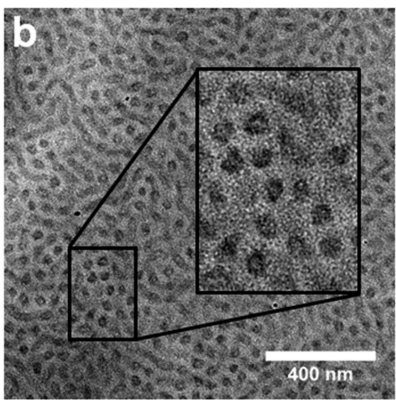


Figure 3. Bright field TEM demonstrates that cylindrical microdomains are formed at $\varphi_{P3EHT} = 0.38$ (a) and $\varphi_{P3EHT} = 0.21$ (b). Zoomed-in sections highlight the visualization of crystallites via selective RuO₄ staining. Upon visual inspection, domains have been deformed away from being round by crystallization. The extent of deformation is greater in the larger P3EHT volume fraction material.

SAXS/WAXS of shear-aligned materials is leveraged. The polymer is first shear-aligned via a channel flow die.⁴⁸ Shear-aligned cylinders adopt a uniaxial symmetry as confirmed by SAXS both perpendicular to (Figure 4a) and along (Figure 4b)

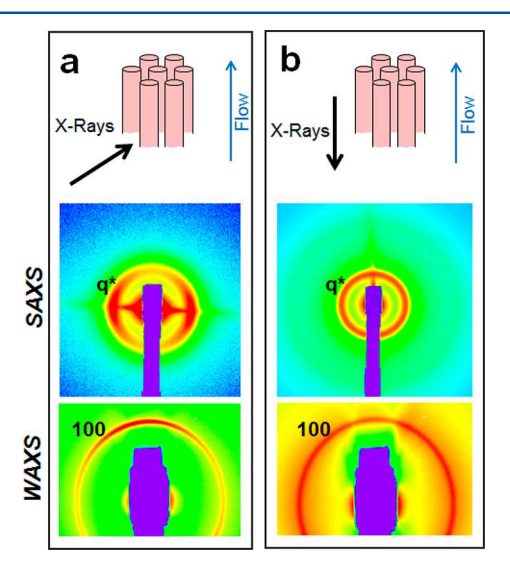


Figure 4. 2-D SAXS/WAXS of aligned cylinder-forming P3EHT-*b*-PMA 8.3K/31.2K. Only 200° of WAXS was available. The 100 WAXS peak corresponds to alkyl chain stacking; the relative orientation in (a) shows that alkyl chain stacking occurs preferentially vertically up the cylinders. In (b) the isotropic scattering in both SAXS and WAXS implies that no preferential crystallite orientation occurs in the cylinder cross section. Cylinders align along the flow direction of the channel flow die and are perpendicular to the constraint direction. 48

the flow direction. Complementary WAXS in these geometries indicates that the preferential orientation of the 100 (alkyl chain stacking) crystal direction is along the long axis of the confined cylinders, and there is no preferred crystalline orientation at the cylinder cross section.

This preferred orientation is initially surprising given that the π -stacking crystal growth is commonly considered to be the strongest direction of crystallite growth in poly(3-alkylthiophenes) and the driving force for fibril formation. Furthermore, this implies that π -stacking occurs primarily across the shortaxis of the cylindrical morphologies. Notably for all diblock morphologies the area per chain at the interfaces significantly decreases upon crystallization due to both (1) the preference

for individual chains to extend upon crystallization and (2) the densification of P3EHT upon crystallization. Both the π stacking and the alkyl chain stacking directions of the crystallite extend perpendicular to the intersection of the P3EHT chain with the microdomain interface. The P3EHT crystal structure contains a fundamental asymmetry in chain-chain distance in the two different packing directions. Assuming chains extend across the entire domain, the average interfacial chain-chain distance (referring to diblock chains that span the interface) around the circumference of the cylinders is merely 0.97 nm (corresponding to roughly twice the π -stacking distance), while the average interfacial chain-chain distance along the long axis of the cylinders is 2.96 nm (corresponding to approximately double the alkyl chain stacking distance). A discussion of calculations that arrive at these values is in the Supporting Information. Given the chain extension and expansion along the cylinder cross section, the system may minimize further expansion in the cylinder diameter by localizing π -stacking along this dimension. By contrast, symmetry prevents crystallites confined within lamellae from having such preferences.

Cylindrical Confinement Impacts Crystallization Dynamics and Crystallite Population. While crystallite orientation and how crystallites are accommodated are critical to the resulting material properties, confinement within microdomains also has the possibility of impacting the resulting crystallization dynamics and stability. By leveraging controlled crystallization conditions and analyzing the resultant crystallite populations by differential scanning calorimetry, we find that confinement controls the resulting crystallite population and nucleation processes. Under standard conditions—crystallization at 25 °C—the crystallite populations observed by DSC in cylindrically confined P3EHT are immediately distinct from those observed in either lamellar-confined or homopolymer P3EHT. In particular, cylindrically confined P3EHT displays a distinct "two-peak" melting behavior (Figure 6a,b), in contrast to lamellar-confined and homopolymer P3EHT which consistently displays "three-peak" melting. In lamellar-confined and homopolymer P3EHT, these three peaks have been assigned to a combination of (low melting) either a rigid amorphous fraction or secondary crystallization and (high melting) a melt-recrystallization process. 27,28,32 Melt-recrystallization processes result in several features appearing by DSC on melting; in reality, this should be considered a meltrecrystallization-melt process. While the recrystallization may

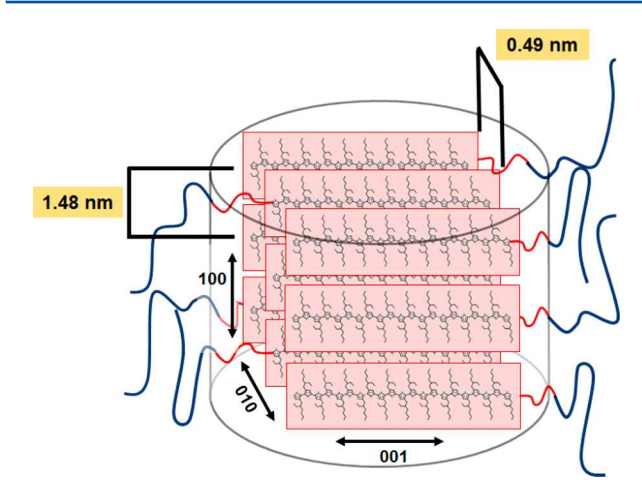


Figure 5. Preferred orientation of P3EHT chains within confined cylinders. Chains are perpendicular to the diblock interface. Given fully extended chains, the system contracts to an area of 1.43 nm² per chain spanning the interface (see Supporting Information for details of the calculation). Within crystals, chains are 1.48 nm apart vertically and 0.49 nm apart horizontally. Note that the crystal structure has been drawn for simplicity; P3EHT adopts a triclinic unit cell with a true alkyl-stacking distance of 1.41 nm and π -stacking distance of 0.51 nm, and the 110 best corresponds to the true π -stacking direction. ¹⁴

be expected to create an exothermic peak, in reality melting and recrystallization often occur simultaneously; the drop in intensity between the initial and final melting peaks corresponds to simultaneous melting and recrystallization, leading to a decreased net heat flow. Studies of the melting-rate dependence of melt—recrystallization in P3EHT help to further clarify these effects. In cylindrically confined P3EHT, the lower melting of these peaks appears to vanish with increasing isothermal crystallization temperature (SI Figure 4) or with controlled annealing conditions (Figure 6c), implying that it corresponds to a less-perfect population of crystallites.

Furthermore, for processing considerations it is important to consider the impact of confinement on the time scales of crystallization. Notably, all P3EHT-b-PMA diblocks require on the order of a week to fully crystallize—considerably longer than the constituent homopolymer P3EHT, which only requires $\sim\!6$ h for reaching a maximum degree of crystallinity for the bulk material. Directly probing the crystallization

kinetics in confinement is challenging due to the long time scales involved; however, significant insight can be gleaned by examining several basic comparisons. In particular, P3EHT-b-PMA cylindrically confined diblocks require considerably more time to crystallize than the corresponding lamellar diblock with identical P3EHT block. Furthermore, even for confined cylinders with identical P3EHT blocks, increasing the relative PMA volume fraction appears to further decrease the crystallization kinetics. The question is whether this is merely a function of slowed dynamics with increasing molecular weight or is truly attributable to shifts in the morphology of confinement. Interestingly, the crystallization dynamics in cylindrical confinement at small P3EHT volume fractions become inaccessibly slow with increasing isothermal crystallization temperature above 35 °C (SI Figure 4). By contrast, P3EHT homopolymer and P3EHT in lamellar confinement both crystallize with accessible kinetics across a range of temperatures from 15 to 55 °C.^{28,32} If the decreased kinetics were due to slowed dynamics alone, the higher crystallization temperatures would be expected to promote, not suppress, crystallization in all cases. Therefore, while we expect the crystallization kinetics can be partially attributed to slowed dynamics, we also attribute it to a decrease in the stability of the crystallite nuclei which grow into the resulting crystallites. Therefore, while individual chain diffusion dynamics may play a role in the slowed kinetics in cylindrical confinement, a significant effect also seems to be the shift in nucleation mechanism.

Previously in the P3EHT homopolymer and in lamellar confinement, it has been shown that increasing the isothermal crystallization temperature improves the resulting degree of crystalline perfection. While this tunability is an important processing consideration for the resulting charge transport properties, in the cylindrically confined system it is not as powerful: the window of accessible crystallization kinetics becomes quite small ($T_{\rm c}$ < 35 °C, as opposed to <55 °C), limiting the degree to which this processing strategy can manipulate the resulting crystallites. Importantly, here it is possible to take advantage of the ease with which these materials exhibit "melt—recrystallization" behavior. The material is first allowed to fully form low-quality crystallites at 25 °C, where nucleation processes are favored. Then, confined cylinders are heated to 65 °C—a temperature at which

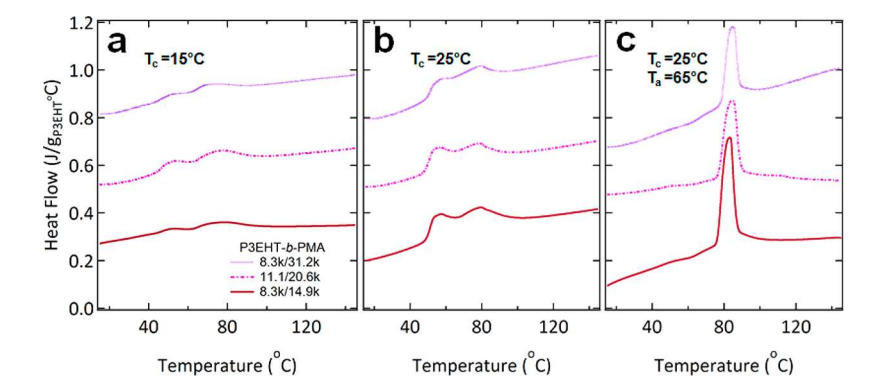


Figure 6. Differential scanning calorimetry of P3EHT crystallized in cylindrical confinement (a) crystallized at 15 °C and (b) crystallized at 25 °C. The weak and multimodal melting peaks on heating are evidence of poor crystallinity, and the melt–recrystallization processes on melting. (c) P3EHT in cylindrical confinement crystallized at 25 °C followed by annealing overnight at 65 °C results in a single population of highly crystalline domains. This approach demonstrates an alternative approach to achieving highly crystalline materials in cylindrical confinement. Directly crystallizing in cylindrical confinement at 65 °C is inaccessibly slow.

crystallites are stable yet could not intrinsically crystallize due to instability of the nuclei. The resulting crystallites form a single uniform population as observed by DSC (Figure 6c). The melting temperature of these crystallites following annealing at 65 °C ($T_{\rm m}=$ ~84 °C for all crystallites) is comparable to the highly perfect crystallites of the constituent homopolymers isothermally crystallized at 55 °C (SI Figure 5) ($T_{\rm m}=$ ~83 °C), which means that the final crystallites even in confinement are highly perfect. Thus, taking advantage of mechanisms for seeding nuclei and then improving crystallinity via annealing steps are promising routes to attaining high-quality crystallites when traditional crystallization routes are unsuccessful.

CONCLUSIONS

Here, the impact of confinement within curved microdomains on the crystallization of conjugated polymers is investigated. Crystallization of conjugated polymers within confinement is impacted by a range of factors, including the interfacial tethering due to the diblock nature of the materials, the mechanical nature of the second block it is attached to, nucleation properties associated with the coherence and volume of confined polymer, and the preference for extended-chain crystallization. This work demonstrates the synthesis of P3EHT-b-PMA diblocks which confine P3EHT within cylindrical microdomains and performs a detailed investigation into how confinement within cylindrical microdomains impacts conjugated polymer crystallization. Importantly, it is observed that confinement templates crystallite orientation such that the 100 (alkyl chain stacking direction) extends down the long axis of the cylinder, while the extended chain and π -stacking direction lie in the cylinder cross section. These observed orientations pose a challenge, as a strategy for templating crystallinity with a faster transport direction, i.e., π stacking, along the long axis of the cylinder must be developed to use these materials as model systems for studying 1-D transport. Furthermore, the combination of TEM and SAXS emphasizes the local deformation that is required to accommodate extended-chain crystallites: not only do the cylinders expand in diameter (as measured by SAXS), but they experience local anisotropic deformations (visible via TEM). Importantly, these confined crystallites also display an apparent change in nucleation mechanism, reducing the ability to tune crystalline perfection merely via isothermal crystallization conditions. Instead, excellent crystallinity is achieved via an initial, accessible crystallization followed by subsequently taking advantage of melt-recrystallization mechanisms. This work examines the unique impacts that crystallization tethered within cylindrical microdomains has on conjugated polymers and highlights both the challenges and promises for achieving additional control over functional polymer nanostructured materials for devices or fundamental charge transport studies.

ASSOCIATED CONTENT

S Supporting Information

The Supporting Information is available free of charge on the ACS Publications website at DOI: 10.1021/acs.macromol.7b01323.

GPC traces, additional TEM, and additional DSC traces (PDF)

AUTHOR INFORMATION

Corresponding Author

*E-mail segalman@engineering.ucsb.edu (R.A.S.).

ORCID ®

Rachel A. Segalman: 0000-0002-4292-5103

Notes

The authors declare no competing financial interest.

ACKNOWLEDGMENTS

We gratefully acknowledge support from the NSF-DMR Polymers Program through grant no. 1608297. This work used user facilities at the Advanced Light Source and at the Stanford Synchrotron Radiation Lightsource, supported by the Director, Office of Science, Office of Basic Energy Sciences, of the U.S. Department of Energy under Contracts DE-AC02-05CH11231 and DE-AC02-76SF00515. We also gratefully acknowledge use of the UCSB MRL Shared Experimental Facilities supported by the MRSEC Program of the NSF under Award DMR 1121053, a member of the NSF-funded Materials Research Facilities Network. We also thank Stephan Kramer for support with TEM imaging and Rachel Behrens for support in the polymer characterization facility.

REFERENCES

- (1) Salleo, A. Charge transport in polymeric transistors. *Mater. Today* **2007**, *10* (3), 38–45.
- (2) Sirringhaus, H.; Tessler, N.; Friend, R. H. Integrated optoelectronic devices based on conjugated polymers. *Science* **1998**, 280 (5370), 1741–1744.
- (3) Thompson, B. C.; Frechet, J. M. J. Organic photovoltaics Polymer-fullerene composite solar cells. *Angew. Chem., Int. Ed.* **2008**, 47 (1), 58–77.
- (4) Himmelberger, S.; Dacuna, J.; Rivnay, J.; Jimison, L. H.; McCarthy-Ward, T.; Heeney, M.; McCulloch, I.; Toney, M. F.; Salleo, A. Effects of Confinement on Microstructure and Charge Transport in High Performance Semicrystalline Polymer Semiconductors. *Adv. Funct. Mater.* **2013**, 23 (16), 2091–2098.
- (5) Jimison, L. H.; Himmelberger, S.; Duong, D. T.; Rivnay, J.; Toney, M. F.; Salleo, A. Vertical Confinement and Interface Effects on the Microstructure and Charge Transport of P3HT Thin Films. *J. Polym. Sci., Part B: Polym. Phys.* **2013**, *51* (7), 611–620.
- (6) Guo, C. H.; Lin, Y. H.; Witman, M. D.; Smith, K. A.; Wang, C.; Hexemer, A.; Strzalka, J.; Gomez, E. D.; Verduzco, R. Conjugated Block Copolymer Photovoltaics with near 3% Efficiency through Microphase Separation. *Nano Lett.* **2013**, *13* (6), 2957–2963.
- (7) Mok, J. W.; Lin, Y. H.; Yager, K. G.; Mohite, A. D.; Nie, W. Y.; Darling, S. B.; Lee, Y.; Gomez, E.; Gosztola, D.; Schaller, R. D.; Verduzco, R. Linking Group Influences Charge Separation and Recombination in All-Conjugated Block Copolymer Photovoltaics. *Adv. Funct. Mater.* **2015**, 25 (35), 5578–5585.
- (8) Hellmann, C.; Treat, N. D.; Scaccabarozzi, A. D.; Hollis, J. R.; Fleischli, F. D.; Bannock, J. H.; de Mello, J.; Michels, J. J.; Kim, J. S.; Stingelin, N. Solution Processing of Polymer Semiconductor: Insulator Blends-Tailored Optical Properties Through Liquid-Liquid Phase Separation Control. *J. Polym. Sci., Part B: Polym. Phys.* **2015**, 53 (4), 304–310.
- (9) Tseng, H. R.; Phan, H.; Luo, C.; Wang, M.; Perez, L. A.; Patel, S. N.; Ying, L.; Kramer, E. J.; Nguyen, T. Q.; Bazan, G. C.; Heeger, A. J. High-Mobility Field-Effect Transistors Fabricated with Macroscopic Aligned Semiconducting Polymers. *Adv. Mater.* **2014**, *26* (19), 2993–2998.
- (10) Patel, S. N.; Su, G. M.; Luo, C.; Wang, M.; Perez, L. A.; Fischer, D. A.; Prendergast, D.; Bazan, G. C.; Heeger, A. J.; Chabinyc, M. L.; Kramer, E. J. NEXAFS Spectroscopy Reveals the Molecular Orientation in Blade-Coated Pyridal[2,1,3]thiadiazole-Containing

Conjugated Polymer Thin Films. *Macromolecules* **2015**, 48 (18), 6606–6616.

- (11) Hu, H. L.; Zhao, K.; Fernandes, N.; Boufflet, P.; Bannock, J. H.; Yu, L. Y.; de Mello, J. C.; Stingelin, N.; Heeney, M.; Giannelis, E. P.; Amassian, A. Entanglements in marginal solutions: a means of tuning pre-aggregation of conjugated polymers with positive implications for charge transport. *J. Mater. Chem. C* **2015**, 3 (28), 7394–7404.
- (12) Kline, R. J.; McGehee, M. D.; Kadnikova, E. N.; Liu, J. S.; Frechet, J. M. J.; Toney, M. F. Dependence of regioregular poly(3-hexylthiophene) film morphology and field-effect mobility on molecular weight. *Macromolecules* **2005**, *38* (8), 3312–3319.
- (13) Duong, D. T.; Ho, V.; Shang, Z. R.; Mollinger, S.; Mannsfeld, S. C. B.; Dacuna, J.; Toney, M. F.; Segalman, R.; Salleo, A. Mechanism of Crystallization and Implications for Charge Transport in Poly(3-ethylhexylthiophene) Thin Films. *Adv. Funct. Mater.* **2014**, *24* (28), 4515–4521.
- (14) Himmelberger, S.; Duong, D. T.; Northrup, J. E.; Rivnay, J.; Koch, F. P. V.; Beckingham, B. S.; Stingelin, N.; Segalman, R. A.; Mannsfeld, S. C. B.; Salleo, A. Role of Side-Chain Branching on Thin-Film Structure and Electronic Properties of Polythiophenes. *Adv. Funct. Mater.* **2015**, 25 (17), 2616–2624.
- (15) Muller, C.; Zhigadlo, N. D.; Kumar, A.; Baklar, M. A.; Karpinski, J.; Smith, P.; Kreouzis, T.; Stingelin, N. Enhanced Charge-Carrier Mobility in High-Pressure-Crystallized Poly(3-hexylthiophene). *Macromolecules* **2011**, *44* (6), 1221–1225.
- (16) Treat, N. D.; Malik, J. A. N.; Reid, O.; Yu, L. Y.; Shuttle, C. G.; Rumbles, G.; Hawker, C. J.; Chabinyc, M. L.; Smith, P.; Stingelin, N. Microstructure formation in molecular and polymer semiconductors assisted by nucleation agents. *Nat. Mater.* **2013**, *12* (7), 628–633.
- (17) Zhang, R.; Li, B.; Iovu, M. C.; Jeffries-EL, M.; Sauve, G.; Cooper, J.; Jia, S. J.; Tristram-Nagle, S.; Smilgies, D. M.; Lambeth, D. N.; McCullough, R. D.; Kowalewski, T. Nanostructure dependence of field-effect mobility in regioregular poly(3-hexylthiophene) thin film field effect transistors. *J. Am. Chem. Soc.* **2006**, *128* (11), 3480–3481.
- (18) Baklar, M.; Barard, S.; Sparrowe, D.; Wilson, R. M.; McCulloch, I.; Heeney, M.; Kreouzis, T.; Stingelin, N. Bulk charge transport in liquid-crystalline polymer semiconductors based on poly(2,5-bis(3-alkylthiophen-2-yl)thieno[3,2-b]thiophene). *Polym. Chem.* **2010**, *1* (9), 1448–1452.
- (19) DeLongchamp, D. M.; Kline, R. J.; Jung, Y.; Lin, E. K.; Fischer, D. A.; Gundlach, D. J.; Cotts, S. K.; Moad, A. J.; Richter, L. J.; Toney, M. F.; Heeney, M.; McCulloch, I. Molecular basis of mesophase ordering in a thiophene-based copolymer. *Macromolecules* **2008**, *41* (15), 5709–5715.
- (20) Sauve, G.; McCullough, R. D. High field-effect mobilities for diblock copolymers of poly(3-hexylthiophene) and poly(methyl acrylate). *Adv. Mater.* **2007**, *19* (14), 1822–1825.
- (21) Sauve, G.; Zhang, R.; Jia, S. J.; Kowalewski, T.; McCullough, R. D. Synthesis, mobility, and conductivity of well-defined regioregular poly(3-hexylthiophene) and diblock copolymers of regioregular poly(3-hexylthiophene). *Proc. SPIE* **2006**, 6336, U164–U172.
- (22) Moon, H. C.; Bae, D.; Kim, J. K. Self-Assembly of Poly(3-dodecylthiophene)-block-poly(methyl methacrylate) Copolymers Driven by Competition between Microphase Separation and Crystallization. Macromolecules 2012, 45 (12), 5201–5207.
- (23) Lim, H.; Chao, C. Y.; Su, W. F. Modulating Crystallinity of Poly(3-hexylthiophene) via Microphase Separation of Poly(3-hexylthiophene)-Polyisoprene Block Copolymers. *Macromolecules* **2015**, 48 (10), 3269–3281.
- (24) Lim, H.; Ho, C. C.; Wu, S. J.; Tsai, H. C.; Su, W. F.; Chao, C. Y. A poly(3-hexylthiophene) block copolymer with macroscopically aligned hierarchical nanostructure induced by mechanical rubbing. *Chem. Commun.* **2013**, *49* (80), 9146–9148.
- (25) Iovu, M. C.; Jeffries-El, M.; Zhang, R.; Kowalewski, T.; Mccullough, R. D. Conducting block copolymer nanowires containing regioregular poly(3-hexylthiophene) and polystyrene. *J. Macromol. Sci., Part A: Pure Appl. Chem.* **2006**, 43 (12), 1991–2000.
- (26) Iovu, M. C.; Zhang, R.; Cooper, J. R.; Smilgies, D. M.; Javier, A. E.; Sheina, E. E.; Kowalewski, T.; McCullough, R. D. Conducting

block copolymers of regioregular poly(3-hexylthiophene) and poly(methacrylates): Electronic materials with variable conductivities and degrees of interfibrillar order. *Macromol. Rapid Commun.* **2007**, 28 (17), 1816–1824.

- (27) Beckingham, B. S.; Ho, V.; Segalman, R. A. Formation of a Rigid Amorphous Fraction in Poly(3-(2 '-ethyl)hexylthiophene). *ACS Macro Lett.* **2014**, 3 (7), 684–688.
- (28) Beckingham, B. S.; Ho, V.; Segalman, R. A. Melting Behavior of Poly(3-(2 '-ethyl)hexylthiophene). *Macromolecules* **2014**, 47 (23), 8305–8310.
- (29) Boudouris, B. W.; Ho, V.; Jimison, L. H.; Toney, M. F.; Salleo, A.; Segalman, R. A. Real-Time Observation of Poly(3-alkylthiophene) Crystallization and Correlation with Transient Optoelectronic Properties. *Macromolecules* **2011**, *44* (17), 6653–6658.
- (30) Ho, V.; Boudouris, B. W.; Segalman, R. A. Tuning Polythiophene Crystallization through Systematic Side Chain Functionalization. *Macromolecules* **2010**, 43 (19), 7895–7899.
- (31) Ho, V.; Boudouris, B. W.; McCulloch, B. L.; Shuttle, C. G.; Burkhardt, M.; Chabinyc, M. L.; Segalman, R. A. Poly(3-alkylthiophene) Diblock Copolymers with Ordered Microstructures and Continuous Semiconducting Pathways. *J. Am. Chem. Soc.* **2011**, 133 (24), 9270–9273.
- (32) Davidson, E. C.; Beckingham, B. S.; Ho, V.; Segalman, R. A. Confined Crystallization in Lamellae Forming Poly(3-(2 '-ethyl)-hexylthiophene) (P3EHT) Block Copolymers. J. Polym. Sci., Part B: Polym. Phys. **2016**, 54 (2), 205–215.
- (33) Martin, J.; Campoy-Quiles, M.; Nogales, A.; Garriga, M.; Alonso, M. I.; Goni, A. R.; Martin-Gonzalez, M. Poly(3-hexylthiophene) nanowires in porous alumina: internal structure under confinement. *Soft Matter* **2014**, *10* (18), 3335–3346.
- (34) Loo, Y. L.; Register, R. A.; Adamson, D. H. Polyethylene crystal orientation induced by block copolymer cylinders. *Macromolecules* **2000**, *33* (22), 8361–8366.
- (35) Quiram, D. J.; Register, R. A.; Marchand, G. R. Crystallization of asymmetric diblock copolymers from microphase-separated melts. *Macromolecules* **1997**, *30* (16), 4551–4558.
- (36) Quiram, D. J.; Register, R. A.; Marchand, G. R.; Adamson, D. H. Chain orientation in block copolymers exhibiting cylindrically confined crystallization. *Macromolecules* **1998**, *31* (15), 4891–4898.
- (37) Quiram, D. J.; Register, R. A.; Marchand, G. R.; Ryan, A. J. Dynamics of structure formation and crystallization in asymmetric diblock copolymers. *Macromolecules* **1997**, *30* (26), 8338–8343.
- (38) Loo, Y. L.; Register, R. A.; Ryan, A. J.; Dee, G. T. Polymer crystallization confined in one, two, or three dimensions. *Macromolecules* **2001**, 34 (26), 8968–8977.
- (39) Hamley, I. W.; Fairclough, J. P. A.; Bates, F. S.; Ryan, A. J. Crystallization thermodynamics and kinetics in semicrystalline diblock copolymers. *Polymer* **1998**, 39 (6–7), 1429–1437.
- (40) Michell, R. M.; Muller, A. J. Confined crystallization of polymeric materials. *Prog. Polym. Sci.* **2016**, 54–55, 183–213.
- (41) Chen, H. L.; Hsiao, S. C.; Lin, T. L.; Yamauchi, K.; Hasegawa, H.; Hashimoto, T. Microdomain-tailored crystallization kinetics of block copolymers. *Macromolecules* **2001**, *34* (4), *671*–*674*.
- (42) Chen, H. L.; Wu, J. C.; Lin, T. L.; Lin, J. S. Crystallization kinetics in microphase-separated poly(ethylene oxide)-block-poly(1.,4-butadiene). *Macromolecules* **2001**, *34* (20), 6936–6944.
- (43) Balsamo, V.; Paolini, Y.; Ronca, G.; Muller, A. J. Crystallization of the polyethylene block in polystyrene-b-polyethylene-b-polycaprolactone triblock copolymers, 1 Self-nucleation behavior. *Macromol. Chem. Phys.* **2000**, *201* (18), 2711–2720.
- (44) Bryant, W. M. D.; Pierce, R. H. H.; Lindegren, C. R.; Roberts, R. Nucleation and Growth of Crystallites in High Polymers Formation of Spherulites. *J. Polym. Sci.* **1955**, *16* (82), 131–142.
- (45) Liu, J. H.; Arif, M.; Zou, J. H.; Khondaker, S. I.; Zhai, L. Controlling Poly(3-hexylthiophene) Crystal Dimension: Nanowhiskers and Nanoribbons. *Macromolecules* **2009**, 42 (24), 9390–9393.

(46) Brunacci, A.; Pedemonte, E.; Turturro, A. Determination of the Equation-of-State Parameters of Poly(Methyl Acrylate). *Polymer* **1992**, 33 (20), 4428–4431.

- (47) Richardson, M. J.; Savill, N. G. Volumetric Properties of Polystyrene Influence of Temperature, Molecular-Weight and Thermal-Treatment. *Polymer* 1977, 18 (1), 3–9.
- (48) Lee, H. H.; Register, R. A.; Hajduk, D. A.; Gruner, S. M. Orientation of triblock copolymers in planar extension. *Polym. Eng. Sci.* **1996**, 36 (10), 1414–1424.
- (49) Huang, T. C.; Toraya, H.; Blanton, T. N.; Wu, Y. X-Ray-Powder Diffraction Analysis of Silver Behenate, a Possible Low-Angle Diffraction Standard. *J. Appl. Crystallogr.* **1993**, *26*, 180–184.
- (50) Ilavsky, J. Nika: software for two-dimensional data reduction. *J. Appl. Crystallogr.* **2012**, *45*, 324–328.
- (51) Zhang, W. L.; Gomez, E. D.; Milner, S. T. Predicting Chain Dimensions of Semiflexible Polymers from Dihedral Potentials. *Macromolecules* **2014**, *47* (18), 6453–6461.
- (52) McCulloch, B.; Ho, V.; Hoarfrost, M.; Stanley, C.; Do, C.; Heller, W. T.; Segalman, R. A. Polymer Chain Shape of Poly(3-alkylthiophenes) in Solution Using Small-Angle Neutron Scattering. *Macromolecules* **2013**, *46* (5), 1899–1907.
- (53) Fetters, L. J.; Lohse, D. J.; Graessley, W. W. Chain dimensions and entanglement spacings in dense macromolecular systems. *J. Polym. Sci., Part B: Polym. Phys.* **1999**, *37* (10), 1023–1033.
- (54) Bates, F. S.; Fredrickson, G. H. Conformational Asymmetry and Polymer-Polymer Thermodynamics. *Macromolecules* **1994**, 27 (4), 1065–1067.
- (55) Almdal, K.; Hillmyer, M. A.; Bates, F. S. Influence of conformational asymmetry on polymer-polymer interactions: An entropic or enthalpic effect? *Macromolecules* **2002**, *35* (20), 7685–7691.
- (56) Matsen, M. W.; Bates, F. S. Conformationally asymmetric block copolymers. J. Polym. Sci., Part B: Polym. Phys. 1997, 35 (6), 945–952.
- (57) Bates, F. S.; Schulz, M. F.; Rosedale, J. H.; Almdal, K. Correlation of Binary Polyolefin Phase-Behavior with Statistical Segment Length Asymmetry. *Macromolecules* **1992**, 25 (20), 5547–5550.
- (58) Bates, F. S.; Schulz, M. F.; Khandpur, A. K.; Forster, S.; Rosedale, J. H.; Almdal, K.; Mortensen, K. Fluctuations, Conformational Asymmetry and Block-Copolymer Phase-Behavior. *Faraday Discuss.* **1994**, *98*, 7–18.
- (59) Olsen, B. D.; Segalman, R. A. Self-assembly of rod-coil block copolymers. *Mater. Sci. Eng., R* **2008**, 62 (2), 37–66.
- (60) Olsen, B. D.; Shah, M.; Ganesan, V.; Segalman, R. A. Universalization of the phase diagram for a model rod-coil diblock copolymer. *Macromolecules* **2008**, *41* (18), 6809–6817.
- (61) Loo, Y. L.; Register, R. A.; Ryan, A. J. Modes of crystallization in block copolymer microdomains: Breakout, templated, and confined. *Macromolecules* **2002**, *35* (6), 2365–2374.
- (62) Loo, Y. L.; Register, R. A.; Adamson, D. H. Direct imaging of polyethylene crystallites within block copolymer microdomains. *J. Polym. Sci., Part B: Polym. Phys.* **2000**, 38 (19), 2564–2570.
- (63) Sirringhaus, H.; Brown, P. J.; Friend, R. H.; Nielsen, M. M.; Bechgaard, K.; Langeveld-Voss, B. M. W.; Spiering, A. J. H.; Janssen, R. A. J.; Meijer, E. W.; Herwig, P.; de Leeuw, D. M. Two-dimensional charge transport in self-organized, high-mobility conjugated polymers. *Nature* 1999, 401 (6754), 685–688.